Geophysical Research Letters

RESEARCH LETTER
10.1029/2020GL087474

Key Points:
- The photosynthetic pathway (C3, C4) impacts the relationship between CO_2 uptake and SIF, which helps to interpret satellite signals
- TROPOMI SIF agrees well with the seasonality of crop gross primary production (GPP) when accounting for C3/C4 fractionation
- TROPOMI SIF is highly correlated with USDA reported crop productivity at the county scale

Supporting Information:
- Supporting Information S1

Correspondence to:
L. He and C. Frankenberg,
cfranken@caltech.edu;
lhe@caltech.edu

Citation:
He, L., Magney, T., Dutta, D., Yin, Y., Köhler, P., Grossmann, K., et al. (2020). From the ground to space: Using solar-induced chlorophyll fluorescence to estimate crop productivity. *Geophysical Research Letters*, *47*, e2020GL087474. https://doi.org/10.1029/2020GL087474

Received 10 FEB 2020
Accepted 4 MAR 2020
Accepted article online 9 MAR 2020

From the Ground to Space: Using Solar-Induced Chlorophyll Fluorescence to Estimate Crop Productivity

Liyin He[1], Troy Magney[1,2], Debsunder Dutta[1,3], Yi Yin[1], Philipp Köhler[1], Katja Grossmann[4,5], Jochen Stutz[4], Christian Dold[6], Jerry Hatfield[6], Kaiyu Guan[7,8], Bin Peng[7,8], and Christian Frankenberg[1,9]

[1]Division of Geological and Planetary Sciences, California Institute of Technology, Pasadena, CA, USA, [2]Now at Department of Plant Sciences, University of California, Davis, CA, USA, [3]Now at Department of Civil Engineering, Indian Institute of Science, Bangalore, India, [4]Department of Atmospheric Sciences, University of California, Los Angeles, CA, USA, [5]Now at Institute of Environmental Physics, University of Heidelberg, Heidelberg, Germany, [6]National Laboratory for Agriculture and the Environment, USDA-ARS, Ames, IA, USA, [7]Department of Natural Resources and Environmental Sciences, University of Illinois at Urbana-Champaign, Urbana, IL, USA, [8]National Center for Supercomputing Applications, University of Illinois at Urbana-Champaign, Urbana, IL, USA, [9]Jet Propulsion Laboratory, California Institute of Technology, Pasadena, CA, USA

Abstract Timely and accurate monitoring of crops is essential for food security. Here, we examine how well solar-induced chlorophyll fluorescence (SIF) can inform crop productivity across the United States. Based on tower-level observations and process-based modeling, we find highly linear gross primary production (GPP):SIF relationships for C4 crops, while C3 crops show some saturation of GPP at high light when SIF continues to increase. C4 crops yield higher GPP:SIF ratios (30–50%) primarily because SIF is most sensitive to the light reactions (does not account for photorespiration). Scaling to the satellite, we compare SIF from the TROPOspheric Monitoring Instrument (TROPOMI) against tower-derived GPP and county-level crop statistics. Temporally, TROPOMI SIF strongly agrees with GPP observations upscaled across a corn and soybean dominated cropland ($R^2 = 0.89$). Spatially, county-level TROPOMI SIF correlates with crop productivity ($R^2 = 0.72$; 0.86 when accounting for planted area and C3/C4 contributions), highlighting the potential of SIF for reliable crop monitoring.

Plain Language Summary Crop monitoring is essential for ensuring food security, but reliable, instantaneous production estimates at the global scale are lacking. The monitoring of crop production in a changing climate is of paramount importance to sustainable food security. Accurate estimates of crop production are dependent on adequately quantifying crop photosynthesis. Our paper demonstrates that solar-induced chlorophyll fluorescence (SIF), an emission of red to far-red light from chlorophyll is highly correlated with crop photosynthesis. We show that a new high spatial resolution satellite SIF data set is highly correlated with crop productivity in the United States, which is benchmarked by the United States Department of Agriculture county-level crop statistics. These results will improve the understanding of crop production and carbon flux over agricultural lands, as well as provide an accurate, large-scale, and timely monitoring method for global crop production estimates.

1. Introduction

Cropping systems not only provide sustenance for the world's human population and livestock, but they also have a major impact on both local climate (Mueller et al., 2016) and the carbon cycle (Peters et al., 2007). Hence, large-scale crop monitoring and yield forecasting are necessary to support food security and to quantify the overall impact on the climate and carbon cycle.

Crop productivity is reliant upon its ability to convert light energy into sugar via photosynthesis. Therefore, a reliable measure of gross primary production (GPP) is a key step toward crop monitoring. Satellite observations have the potential to provide GPP estimates from regional to global scales (Running et al., 2004; Ryu et al., 2019; Turner et al., 2006; Yuan et al., 2007; Zhao et al., 2005). Most remote sensing-based GPP estimates use spectral information in the visible and near infrared (NIR) regions that are related to greenness

(Huete et al., 2002) or thermal (Anderson et al., 2012) and microwave bands, which are sensitive to vegetation/soil water content (Guan et al., 2017; Konings et al., 2017). In most cases, predicting GPP largely depends on empirical estimates of light use efficiency (LUE, efficiency with which absorbed light is used for CO_2 fixation), which is highly uncertain.

The emission of red and far-red light from excited chlorophyll-a molecules, denoted solar-induced chlorophyll fluorescence (SIF), offers a physiologically based GPP proxy, potentially avoiding the need for LUE parameterizations. In fact, an empirical linear scaling between SIF and GPP across various vegetation types under different environmental conditions has already been shown in many studies (Frankenberg et al., 2011; Guanter et al., 2014; Guan et al., 2016; Li et al., 2018; Magney, Bowling, et al., 2019; Smith et al., 2018; Song et al., 2018; Sun et al., 2018; Verma et al., 2017; Wood et al., 2017; Zhang et al., 2016; Zuromski et al., 2018), revealing the potential of SIF to monitor GPP across all spatial scales.

The rationale of linking SIF with crop productivity can be shown using the following equations (Guan et al., 2016):

$$\sum NPP = \sum GPP - \sum Ra = CUE \cdot \sum GPP, \tag{1}$$

$$Crop\ Productivity = \sum NPP \cdot fAG \cdot HI, \tag{2}$$

$$\sum SIF \sim \sum GPP, \tag{3}$$

where $\sum$ means the temporal integration of the variable over the growth period. *NPP* refers to net primary production, calculated as GPP minus the amount of carbon consumed by plants by autotrophic respiration (*Ra*), which includes maintenance and growth respiration. During the growing period, we can assume that growth respiration dominates the *Ra* term, which in theory should scale with *GPP*. *CUE* is the carbon use efficiency, which varies across species and environmental conditions (Amthor, 1989; DeLucia et al., 2007). *fAG* is the fraction of the aboveground to total biomass and *HI* is the harvest index—the mass of harvested grain divided by total aboveground biomass. Both *fAG* and *HI* are related to the crop type and environmental conditions but are usually treated as constant parameters for individual crops. These equations exhibit the underlying relationship among SIF, NPP, GPP, and crop productivity and show that even if GPP and SIF are perfectly correlated, variations in *CUE*, *fAG*, and *HI* can still impact the relationship of SIF to crop productivity.

Some efforts have been made to explore the potential of satellite SIF in estimating crop productivity. Guanter et al. (2014) found that the highest SIF values observed from the Global Ozone Monitoring Experiment-2 (GOME-2) satellite are associated with the Corn Belt in the United States Midwest. In addition, SIF captured the photosynthetic activity over highly productive croplands, while traditional vegetation indices (VIs) show saturation effects in dense canopies. In some cropping systems, however, the use of NIRv (Badgley et al., 2017) might track productivity quite well (Dechant et al., 2019) but may be less sensitive to rapid changes in PSII operating efficiency. Thus, SIF has its own unique advantage to track crop photosynthesis over VIs. Guan et al. (2016) used GOME-2 SIF as an approximation of photosynthetic electron transport rate (ETR) to derive GPP and crop yield, which has shown a significant improvement in county-level crop yield estimates. Zhang et al. (2014) proposed the utility of space-based SIF measurements, combined with a process-based model, to estimate the photosynthetic capacity over six crop flux sites in the United States. However, direct comparisons of SIF and crop yields have been restricted by the coarse spatial resolution of available satellite SIF measurements. In the United States, the average area of counties that are predominantly agricultural is ~1,700 km^2, with the smallest one ~430 km^2. A single GOME-2 footprint (80 km × 40 km) thus covers several counties, making it challenging to compare SIF with the benchmark of county-level annual crop statistics from the National Agricultural Statistics Service (NASS) of the United States Department of Agriculture (USDA). Fine spatial resolution (1.3 km × 2.25 km) SIF data from the Orbiting Carbon Observatory (OCO-2) has been available since September 2014 (Frankenberg et al., 2015; Sun et al., 2017) but does not provide contiguous spatial coverage. To fill this knowledge gap, we leverage SIF inferred from measurements of the TROPOspheric Monitoring Instrument (TROPOMI), with an unprecedented spatial resolution (up to 7 km × 3.5 km) and near-global daily coverage (Köhler et al., 2018), which allows us to achieve robust SIF averages for individual counties.

A thorough understanding of the relationship between SIF and GPP and how it might vary depending on photosynthetic pathway (C3, C4) is important to achieve accurate estimates of crop photosynthesis from SIF. Some studies found stronger relationships between SIF and absorbed light by chlorophyll, than GPP (Li et al., 2020; Yang et al., 2018). As SIF emanates from the light reactions of photosynthesis, it is expected to be more closely related to the ETR in photosystem II than to GPP (Frankenberg et al., 2011; Gu et al., 2019; Porcar-Castell et al., 2014). Thus, the GPP:SIF ratio should vary between C3 and C4 photosynthetic pathways (Gu et al., 2019; Guan et al., 2016; Porcar-Castell et al., 2014), because it is important to know how efficiently electrons from the light reactions are used for carbon fixation. This is fundamentally different for C3 and C4 plants, with the latter inhibiting photorespiration, which generally leads to a higher and less variable efficiency. Typical C3 crops include soybeans, wheat, barley, oats, and rice, whereas typical C4 crops include corn, sugarcane, and sorghum. Several recent studies point to a different GPP:SIF ratio for C3 and C4 plants (Li et al., 2018; Liu et al., 2017; Wood et al., 2017); however, there is still limited understanding of how exactly these mechanisms influence the GPP:SIF relationship across time and space. To fill this knowledge gap, we include both field measurements and a biophysical model to explain the discrepancies of GPP:SIF of C3 and C4 crops and use this to inform our interpretation of the satellite data.

In this paper, the objectives are to (i) compare observed and modeled GPP:SIF relationships for C3 and C4 crops at site level, (ii) examine whether aggregated TROPOMI SIF at local (10 km) scales can represent the seasonality of GPP observations over homogenous croplands, and (iii) evaluate how well aggregated TROPOMI SIF at the county level can be used to estimate crop productivity and NPP in the United States.

2. Data and Methods

2.1. Site-Level SIF and GPP Observations

2.1.1. Eddy-Covariance GPP

In this paper, eddy-covariance (EC) data were collected at long-term and well-characterized USDA agricultural flux towers within C3 (soybeans, *Glycine max* L. Merr.) and C4 (corn, *Zea mays* L.) cropping systems in central Iowa. Specific sites are Brooks Field (41.974536°N, −93.693711°W) and Coles Field (42.488414°N, −93.522582°W) for the PhotoSpec comparison in 2017 as well as two nearby towers at Coles Field covering soy (42.488414°N, −93.522582°W) and corn (42.481677°N, −93.523521°W) for the TROPOMI comparison in 2018. These farming systems are typical for those in the Upper Midwest corn belt (more details in Dold et al., 2017, 2019). Data were excluded under unfavorable weather conditions (e.g., rainfall, low wind turbulence, and high humidity) (Baker & Griffis, 2005), screened for outliers (Dold et al., 2017), and gap-filled. Turbulent CO_2 fluxes were computed using the EC method (Burba, 2013), and then net ecosystem exchange was partitioned into GPP and ecosystem respiration (Re). Note that we do not have overlapping data sets of TROPOMI, PhotoSpec and EC systems; thus, the EC to PhotoSpec comparison is limited to 2017 and the EC to TROPOMI comparison to 2018.

2.1.2. PhotoSpec SIF

We installed two PhotoSpec instruments in a soybean (Brooks Field, 41.974203°N, −93.695839°W) and corn field (Coles Field, 42.48655°N, −93.52641°W) in central Iowa following planting in late May 2017 and measured SIF until harvest in September 2017 (Magney, Frankenberg, et al., 2019). PhotoSpec consists of a 2D scanning telescope to guide reflected radiances into a set of high-resolution spectrometers (Grossmann et al., 2018) to infer SIF using the solar Fraunhofer line in-filling technique, similar to all current satellite retrievals. The scanning telescope was placed atop a 7-m tower, and we calculate a "canopy average" of all viewing angles at an hourly time step to match the temporal resolution of flux tower data (following Magney, Frankenberg, et al., 2019). Because the scanning telescope revisits every measuring point within an hour, this canopy average is more representative of a hemispherical sensor with a footprint of a few meters around the tower (an average of all viewing directions). Due to the narrow field of view of PhotoSpec, we can isolate between vegetation and nonvegetation signals, where we have determined NDVI at 0.6 to be sufficient for the definition of the peak growing season, when our analysis was conducted (as can be seen in Figure S1 in the supporting information, where the rows can be seen early in the season). Notably, while the escape ratio and angular dependencies are an important consideration for tower-based SIF measurements (Zeng et al., 2019), this makes little difference in our study for the canopy structure is relatively stable during the peaking growing season. More details on PhotoSpec retrievals and instrument specifications can be found in Grossmann et al. (2018) and Magney, Frankenberg, et al. (2019).

2.2. TROPOMI SIF

On 13 October 2017, the TROPOMI instrument onboard the European Sentinel-5 Precursor satellite was launched. TROPOMI is a multiband push-broom imaging grating spectrometer, which also covers the far-red part of the SIF emission spectrum (Köhler et al., 2018). The SIF retrieval window ranges from 743 to 758 nm, a subset of TROPOMI's band 6 (725–775 nm). A daily correction factor is applied to convert instantaneous SIF to a daily average (following Frankenberg et al., 2011).

For the comparison with GPP observations, we extracted TROPOMI SIF within +/−10 km of two nearby flux towers and applied a +/−4-day moving average, sampled every 4 days. The agricultural cover is quite homogeneous within +/−10 km, with ~58% corn and ~30% soybeans derived from the 30-m cropland data layer (CDL; https://nassgeodata.gmu.edu/CropScape/) (Figure S2). Since TROPOMI SIF represents an average of all crops within the sampling area, we assume a ⅔:⅓ weighted average of flux tower GPP for corn and soy, respectively.

For the comparison with county-level crop statistics reported by USDA NASS, we aggregated SIF at the county scale, yielding on average 700 TROPOMI soundings per month for counties with >45% planted areas. The planted ratio of each county is shown in Figure S3.

2.3. Crop Statistics From USDA NASS

We obtained the county-level total crop production and planted area for individual crop types from the USDA NASS Quick Stats Database (quickstats.nass.usda.gov). In most studies, crop yield refers to the amount of grain per unit of harvested land area per crop (Fischer, 2015). Therefore, it is associated with accumulated NPP weighted by aboveground biomass during the crop growth season (Lobell et al., 2002). Thus, NPP acts as a bridge to link crop statistics with satellite observations (Smith et al., 2014).

We used crop production and acreage for individual crop types to calculate county-level crop productivity as $\frac{\text{total crop production}}{\text{total county area}}$. From a physical perspective, this definition is more comparable with the county-level aggregated satellite TROPOMI SIF, since satellite SIF records represent the entire footprint, regardless of land type.

Following Lobell et al. (2002), Guan et al. (2016), and Guan et al. (2017), we converted crop productivity to NPP at the county level:

$$NPP\left(\frac{gC}{m^2}\right) = \sum_{i=1}^{N} \frac{P_i \cdot MRP_i \cdot (1-MC_i) \cdot 0.45 \frac{gC}{C}}{HI_i \cdot fAG_i} / total\ county\ area, \tag{4}$$

$$= \sum_{i=1}^{N} \frac{Y_i \cdot MRP_i \cdot (1-MC_i) \cdot 0.45 \frac{gC}{C}}{HI_i \cdot fAG_i}, \tag{5}$$

where i represents the crop type (dominated by corn and soybean here), P the reported crop production, MRP the mass per unit of report production, MC the moisture content, and Y the crop productivity based on the definition given before. The list of fAG and HI of common crops can be found in Lobell et al. (2002) and Guan et al. (2016) (see Table S1).

2.4. Site-Level GPP and SIF Modeling

We use the Soil Canopy Observation, Photochemistry and Energy fluxes (SCOPE) model, a 1D integrated radiative transfer and energy balance model, to simulate photosynthesis, fluorescence, the surface energy balance, and reflectance/emission spectra at leaf and canopy scales (van der Tol et al., 2009). This mechanistic model helps to understand the connection between SIF, GPP, quantum yield of photosystem II (PSII) ($PSII_{\text{yield}}$) and actual ETR (Ja) under different environmental conditions for C3 and C4 plants. We modeled GPP and SIF at nadir viewing using SCOPE at two flux tower sites with concurrent PhotoSpec and GPP observations. We used available meteorological data from the flux tower (i.e., incoming shortwave and longwave radiation, air temperature, ambient atmospheric pressure, vapor pressure, and wind speed) and optimized canopy parameters (leaf area index, V_{CMAX}, and Chl content) via a Bayesian inversion system (Dutta et al., 2019).

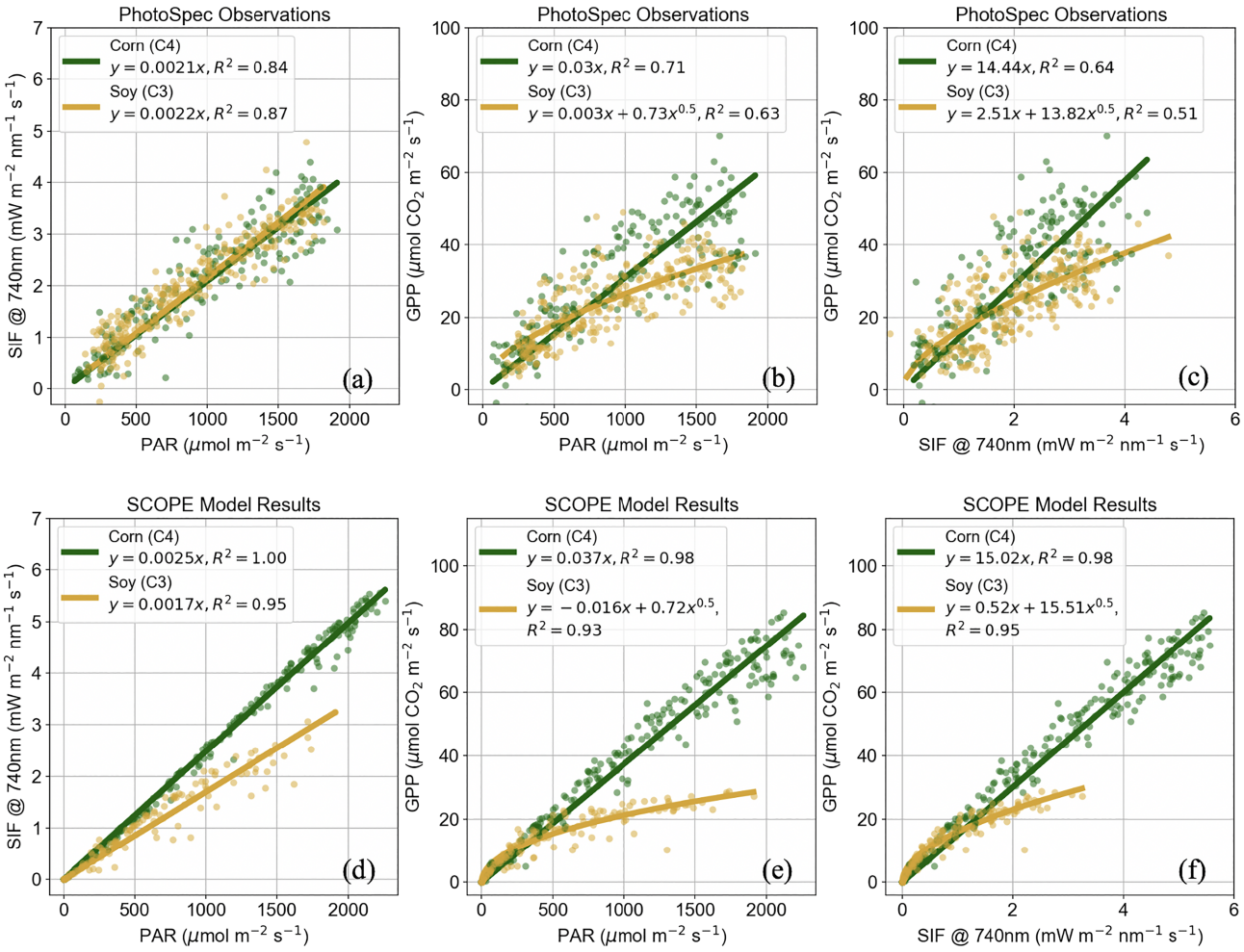

Figure 1. Canopy-scale relationships in the peak growing season (DOY 175-190 for corn and 210-235 for soybean) based on hourly averaged data from PhotoSpec for soybean (gold) and corn (green): (a) SIF:PAR, (b) GPP:PAR, and (c) GPP:SIF for both soybeans and corn. SCOPE modeled relationships are for the same time-periods and based on hourly averaged data for soybean and corn: (d) SIF:PAR, (e) GPP:PAR, and (f) GPP:SIF. The results of PhotoSpec-measured relative SIF, which is normalized by incoming NIR-reflected radiance to reduce the effects of structural and bidirectional reflectance of the signal (Yang et al., 2018), are shown in Figure S4.

3. Results and Discussion

3.1. Observed and Modeled GPP:SIF for C3 and C4 at the Site Level

We compared ground-based PhotoSpec SIF measurements throughout the peak growing season in both C3 (soybean) and C4 (corn) crops with flux tower GPP as well as photosynthetically active radiation (PAR) (Figures 1a–1c). The peak growing season is defined as DOY 210-235 for soybean and DOY 175-190 for corn. Here, hourly SIF is linearly correlated with PAR for soybean ($R^2 = 0.87$) and corn ($R^2 = 0.84$), with negligible differences in the SIF:PAR ratio (Figure 1a). This indicates that during the peak growing season in both agricultural sites, SIF is mostly driven by incident radiation and exhibits negligible differences due to the fluorescence yield. To first order, we expect SIF to be tightly related to PAR in systems where there is little stress (i.e., low variations in SIF_{yield}), which can be expected in highly efficient agricultural areas. Little apparent stress is also indicated by the canopy-scale light response curve of GPP vs. PAR (Figure 1b), with a near-linear relationship for corn and some saturation effects for soybean at higher light levels. Consequently, we found that hourly averaged SIF is strongly correlated with GPP in both soybean ($R^2 = 0.51$) and corn ($R^2 = 0.64$), however, with a larger GPP:SIF ratio observed for corn, leading to roughly a 30% higher GPP per unit SIF in corn at higher light levels (Figure 1c). This implies that the light-use efficiency of corn is higher than that of soybean, due to the evolved mechanism to concentrate CO_2 at the

rubisco site and thereby minimize photorespiration as well as the occurrence of carboxylation limited photosynthetic rates in C4 plants.

To test whether the GPP:SIF relationship observed in the field is consistent with what is expected from biophysical models, we compared the simulated far-red SIF at 740 nm and GPP against PAR using SCOPE (Figures 1d– 1f). For both soybean and corn, the PAR:SIF relationship is highly linear yet with slightly different slopes (Figure 1d). In the light response curve for GPP (Figure 1e), soybean GPP saturates at higher light levels, when the rate of photosynthesis is limited by the carboxylation rate. Corn remains highly linear even at high light levels, resulting in a more linear GPP:SIF relationship. Apart from the high SIF values modeled for corn leading to diverging SIF:PAR relationships between corn and soy, these simulations are broadly consistent with our observational evidence. We found that the high SIF to PAR slope for C4 is likely related to how SCOPE computes the $PSII_{\text{yield}}$ for C4 plants, which are in the range of a maximum SIF_{yield} given by the $PSII_{\text{yield}}$:SIF_{yield} parameterization (Van der Tol et al., 2014). Our canopy spectrometer data supports this, as we observe similar SIF yields for C3 and C4 crops. The overly high modeled SIF values as well as the inconsistency with our field measurements point to an overestimation in the SIF_{yield} for C4 plants in the SCOPE model. Apart from that, the measurement and modeling perspective agree very well.

Both our observations at the site level as well as the SCOPE modeling results showed that the GPP:SIF relationship is more linear for C4 than C3 plants. It is well established that SIF is a better proxy for the actual ETR (Ja) than for GPP, which requires us to separate C3 and C4 photosynthetic mechanisms if we use Ja to estimate GPP. The explicit relationships among the four variables, SIF, Ja, $PSII_{\text{yield}}$, and SIF_{yield}, can be described as follows (Gu et al., 2019; Porcar-Castell et al., 2014):

$$Ja = \Phi_{\text{PSII}} \cdot \beta \cdot APAR_{\text{green}}, \tag{6}$$

$$SIF = \Phi_{\text{SIF}} \cdot \beta \cdot \varepsilon \cdot APAR_{\text{green}}, \tag{7}$$

where Φ_{PSII} and Φ_{SIF} is the quantum yield of PSII and SIF, respectively; $APAR_{\text{green}}$ is absorbed PAR by green elements (Gitelson & Gamon, 2015); β is the fraction of $APAR_{\text{green}}$ allocated to PSII; ε is the escape probability of fluorescence from the canopy (Zeng et al., 2019). Here, we neglect variations in the canopy structure and thus ε as we focus on the peak growing season, where we observe little structural change (Figure S1).

Combing 6 and 7, we obtain

$$\frac{Ja}{SIF} \sim \frac{\Phi_{\text{PSII}}}{\Phi_{\text{SIF}}}, \tag{8}$$

which demonstrates that Ja:SIF is determined by Φ_{PSII} and Φ_{SIF}, which is dependent on environmental conditions (e.g., light intensity, drought, and heat stress). The less Φ_{PSII} is varying—as is often the case for highly efficient crops—the more constant and linear the SIF to Ja relationship is. Leaf-level measurements have been used to derive the empirical relationship between Φ_{PSII} and Φ_{SIF} (Lee et al., 2013; Van der Tol et al., 2014). For example, Flexas et al. (2002) found that for under stress, Φ_{PSII} and Φ_{SIF} are usually positively correlated if substantial nonphotochemical quenching exists. At the canopy level, Φ_{PSII} and Φ_{SIF} are mostly positively correlated at the seasonal scale (Porcar-Castell et al., 2014; Song et al., 2018; Verma et al., 2017; Yang et al., 2015; Zhang et al., 2016), mainly due to averaging effects of the canopy, which integrates over a variety of Φ_{PSII} and Φ_{SIF} values for all leaves (similar to our PhotoSpec observations).

The linkage between GPP and Ja depends on the photosynthetic pathway (Collatz et al., 1992; Farquhar et al., 1980):

$$GPP = \frac{Ja \cdot \left(C_c - \Gamma^*\right)}{4C_c + 8\Gamma^*} \text{ for C3}, \tag{9}$$

$$GPP \approx \frac{Ja}{6} \quad \text{for C4}, \tag{10}$$

where C_c is chloroplast CO_2 partial pressure and Γ^* is chloroplastic photorespiratory CO_2 compensation point. Comparing 9 and 10, for C3 plants, an additional nonlinearity in GPP:Ja arises, which is attributed

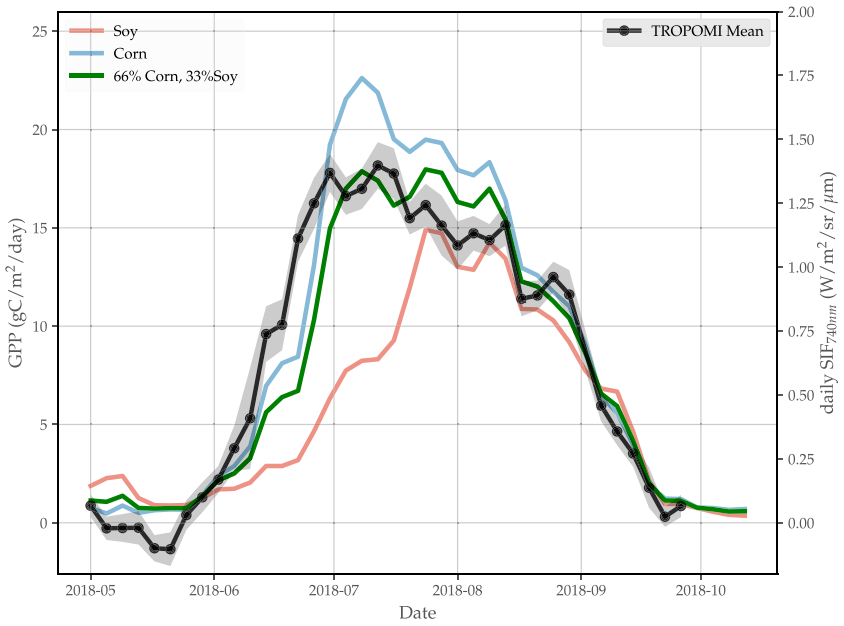

Figure 2. The 2018 seasonal cycle of flux tower GPP for soybeans and corn in Iowa and TROPOMI SIF (within +/−0.1° latitude and longitude, shaded area showing 2 sigma uncertainty range). A moving average of +/−4 days and 4-day sampling interval is applied to both data sets. The upscaled GPP (green) is approximated by a weighted average of ⅔ corn and ⅓ soy contributions, determined by computing crop fraction within +/−0.1° (in total, 88% of this area is covered by either corn and soybean).

to the varying fraction of electrons used in photorespiration. Due to the lack of photorespiration in C4 plants, the relationship between Ja and GPP is strictly linear. For the same reason, the conversion factor from Ja to GPP is mostly higher for C4 than C3 plants, as about ⅓ of the ETR is wasted in photorespiration in C3 plants. Since SIF is mostly proportional to Ja, 9 and 10 directly explain the more linear behavior and steeper GPP:SIF slope for C4 versus C3 plants. It should be noted that at high C_c values, the slope for C3 plants can be steeper (e.g., at low light levels). In general, variations in the GPP:SIF scaling at the leaf scale can thus be attributed to two different effects: (i) variations in the ratio of Φ_{PSII} and Φ_{SIF} in the light reactions as well as (ii) the scaling from Ja to GPP, which depends on the photosynthetic pathway.

3.2. Consistent Seasonal Cycle Seen by TROPOMI SIF and Field GPP Measurements

Here, we evaluate how well TROPOMI SIF represents local GPP patterns in a corn/soybean dominated area in Iowa during the growing season of 2018. The seasonal cycle of footprint-level TROPOMI SIF and flux tower GPP at both soybean and corn sites is shown in Figure 2. Corn GPP increases more rapidly and reaches its maximum of ~25 gC/m^2/day around 10 July, while soybean GPP approaches maximum of ~15 gC/m^2/day more gradually, around 20 July. As mentioned in Section 2.2, TROPOMI SIF represents an average of all crops in the area, for which we calculate the weighted average of GPP assuming a ⅔:⅓ contribution of corn and soy, respectively. There is strong agreement between TROPOMI SIF and the weighted area-averaged GPP estimate ($R^2 = 0.89$) (Figure 2), motivating our use of TROPOMI SIF in large-scale crop monitoring. In particular, the GPP:SIF ratio at both satellite and flux tower scales is consistent—around 12 (gC/m^2/day)/(W/m^2/μm/sr). While there is close correspondence between SIF and GPP during senescence, there is a small mismatch early in the growing season, which could be explained by (1) fewer TROPOMI observations due to increased cloud cover during this time of year (see Figure S5), (2) different planting and emergence dates within the satellite footprint, and (3) potentially higher SIF escape probabilities at the beginning of the season as the canopy is more open at that stage. We also did not find any apparent viewing angle dependent behavior in the TROPOMI data sets (see Figure S5). Importantly, it should be noted that this is the first time that satellite-based SIF can be compared with GPP at weekly temporal resolution and ~10 km spatial scales—a significant improvement over previous satellites providing monthly data at 0.5° resolution.

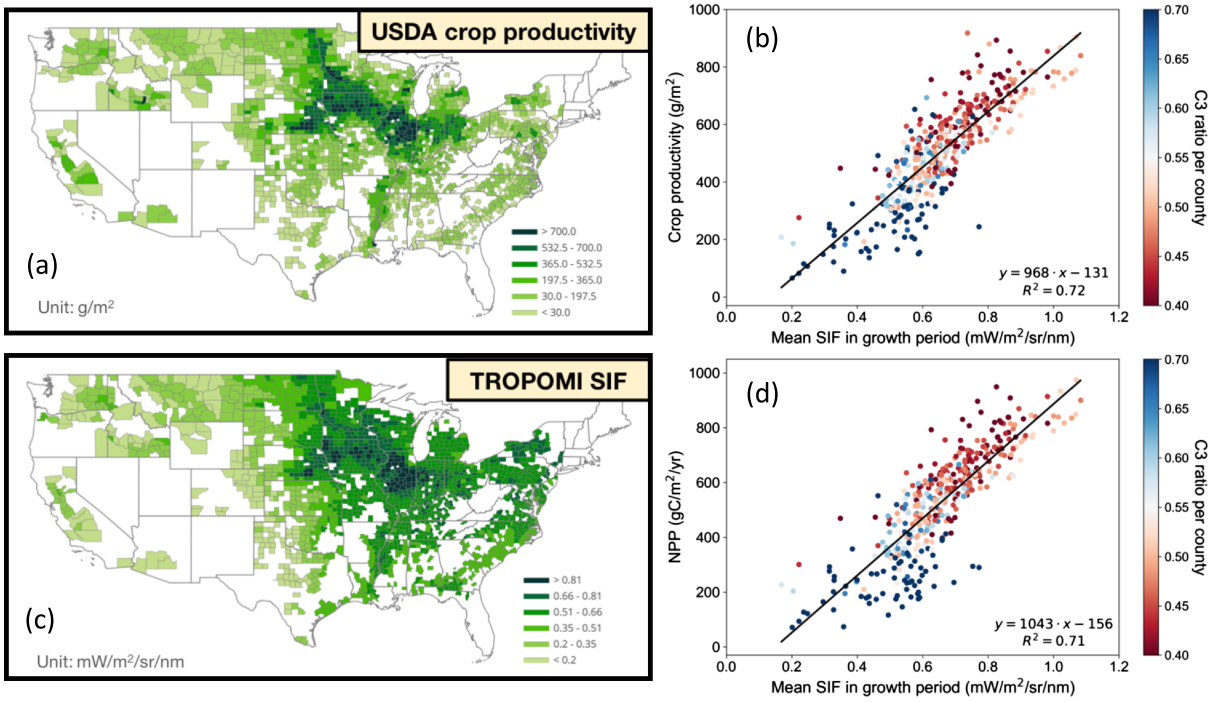

Figure 3. Spatial pattern of county-scale (a) crop productivity derived from USDA NASS and (c) average TROPOMI SIF during the growth period of 2018. In counties with planted area >45%, the relationship of (b) crop productivity: SIF and (d) NPP:SIF. The color scheme represents the relative fraction of C3 crops, with blue meaning more C3 and red means more C4. The maps of C3 and C4 crops distributions are shown in Figure S6. The growth period here is defined as the time when SIF exceeds 10% of max (SIF) within a year. The results are robust with different thresholds defining the growing season (see Figure S7**)** and TROPOMI relative SIF (see Figure S8).

Tower-level SIF was not included in this comparison as there was no temporal overlap between tower SIF data and TROPOMI in 2018. In recent years, more ground-based SIF measurements have become available (Dechant et al., 2019; Du et al., 2019; Grossmann et al., 2018; Li et al., 2020; Magney, Frankenberg, et al., 2019; Miao et al., 2018; Zhang et al., 2019; Yang et al., 2015; Yang et al., 2018), which will help disentangle various factors (e.g., view angles, canopy structure, and overpass times) that might also impact the SIF to GPP relationship.

3.3. Spatial Correlation Between County-Level TROPOMI SIF and Crop Productivity

Here, we focus on the county level in the United States to evaluate the capability of using TROPOMI SIF to predict crop productivity. We define the growth period for each county as the period in which SIF exceeds 10% of its peak value within the year. The spatial pattern of crop productivity and the average growing-season TROPOMI SIF of 2018 is shown in Figures 3a and 3c. The SIF map closely matches the NASS yield-based NPP pattern in the Corn Belt, the most dominant region of corn/soybean staple crop production in the United States. For counties with >45% planted areas, we found that crop productivity and converted NPP are both highly correlated with SIF, with $R^2 = 0.72$ and $R^2 = 0.71$, respectively (Figures 3b and 3d). As discussed previously, crop productivity: SIF and NPP:SIF relationships are not identical for C3 and C4 crops. At the same level of SIF, higher crop productivity and NPP are observed for counties with more C4, which is expected based on the ground-based measurements and modeling results (Sections 3.1). In contrast to the nonlinear pattern observed for temporal variations at the site level, spatial variations in the county-level analysis are more linear. The main reason is that the nonlinear pattern is only apparent at high light levels. In contrast, the spatial correlation is discussed for seasonal averages, in which the impact of high light levels is smoothed out.

In theory, crop productivity is associated with temporally integrated net photosynthesis over the growing season. Therefore, we also tested the correlation between crop productivity and the corresponding NPP

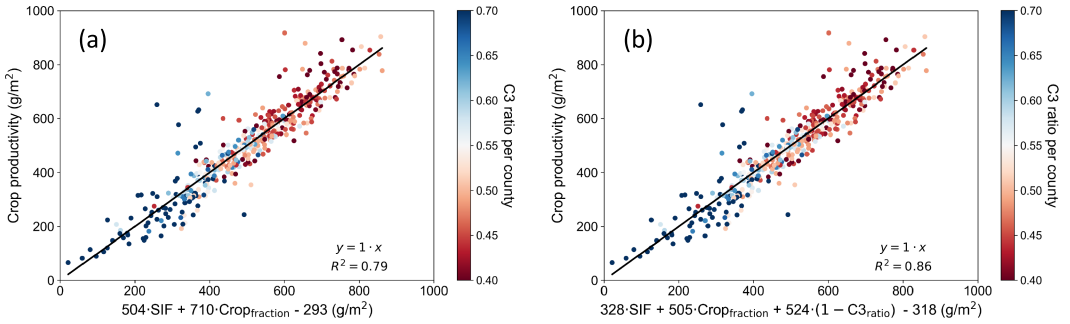

Figure 4. The relationships between true crop productivity and predicted crop productivity using multiple linear regression based on variables (a) SIF and crop fraction per county and (b) SIF, crop fraction, and relative C3 ratio per county.

against integrated SIF over the growing period. We found that the crop productivity:integrated SIF and NPP:integrated SIF correlations are still consistent and robust yet weaker than when using the average growing season SIF (see Figure S9).

Overall, the crop productivity (NPP):SIF relationship at the county level is almost linear. This is likely due to the high efficiency of crops (generally high photosynthetic yields) as well as large contributions from C4 crops, where the relationship is more linear. In addition, crop productivity (NPP):SIF ratio is 25–50% higher for C4 than C3, which is consistent with ground-based measurements and modeling outputs in Sections 3.1. Including results from field measurements (PhotoSpec) and a biophysical model (SCOPE) give us more confidence in explaining the discrepancies between C3 and C4 crops and the associated GPP:SIF relationship. A more detailed understanding of the GPP:SIF slope for different crops at different environmental conditions based on field-level measurements would help us to better estimate NPP:SIF for a variety of crops and ultimately improve the prediction of crop productivity at the global scale, where ground-based measurements are lacking.

3.4. Improving the Productivity Prediction Performance Using Additional Information

Although crop productivity can be estimated with SIF observations alone, we can further improve the performance by adding two other explanatory variables, which are easily accessible: planted area fraction per county ($Crop_{fraction}$) and fraction of C3 plants per county ($C3_{ratio}$). The SIF signal from crops will be dampened if the planted area fraction is low, and a correction factor should be considered between C4 and C3, since higher productivity is expected for C4 at the same level of SIF. Here, we fit the two multiple linear regression models for crop productivity based on (i) SIF and $Crop_{fraction}$ (ii) SIF, $Crop_{fraction}$, and $C3_{ratio}$, (Figure 4). With the added information of $Crop_{fraction}$, R^2 improved from 0.72 to 0.79, and adding the $C3_{ratio}$, R^2 improved to 0.86 (Figures 3 and 4), which also converges into a more normal distribution of the residuals for C3 and C4 dominated counties around the line of best fit. This behavior is consistent with our field-level measurements and modeling, given us mechanistic confidence in such an approach.

It should be noted that we currently use several assumptions and do not use any model information for this upscaling approach. For instance, we assume that respiration scales with GPP, which results in a linear scaling of GPP to NPP. Notably, other growing season environmental conditions (temperature, vapor pressure deficit, and soil moisture) as well as canopy structure and associated variations in the escape probability of SIF could have an impact on our interpretation of the SIF signal. Theoretically, however, SIF contains the information on environmental conditions and tracks GPP variations better than traditional reflectance-based VIs (e.g., NDVI), though its response to stress is weaker than for GPP (or LUE) (Magney et al., 2017; Van der Tol et al., 2014). Additionally, HI, the process of plant NPP converting to ultimate grain yield, which is also controlled by reproductive processes and environmental conditions during grain fill, is an important consideration. Despite this, it is hard to justify adding more complexity to the analysis given the already strong empirical linear relationship between crop NPP and SIF.

3.5. Toward Finer-Resolution Crop Productivity Estimates

Our SIF-only-based crop productivity proxy approach achieved robust and reliable performance over agriculture dominated counties in the United States. To fully exploit the potential of this approach in other

regions of the world, especially for small-scale, diverse, and fragmented agricultural fields, high spatially and temporally resolved remote sensing data sets will be required. This is still challenging for current satellite SIF products (e.g., short record of TROPOMI, sparse spatiotemporal sampling of OCO-2 and large footprint of GOME-2). Recently, some machine learning-based long-term SIF products of high spatiotemporal resolution have been developed (e.g., CSIF, GOSIF, RSIF, and SIF_{oco2}) based on satellite SIF, high-resolution spectral information, and meteorology data (Gentine & Alemohammad, 2018; Yu et al., 2019; Zhang et al., 2018; Li & Xiao, 2019; Turner et al., 2020). Future work across all scales will be needed to test the long-term performance of SIF products on the global scale, particularly as we link these measurements to photosynthesis (Ryu et al., 2019). A combination of high-resolution reflectance-based remote sensing products and crop models (Jin et al., 2017; Lobell et al., 2015) has already shown great potential in fine-scale yield estimates.

4. Conclusions

We investigated the GPP:SIF relationship of crops from ground-based measurements and validated the biophysics with model runs for C3 and C4 crops at two field sites in the Upper Midwest corn belt of the United States during the 2017 growing season. Generally, we find a linear GPP:SIF relationship except for high-light levels when GPP starts to saturate, whereas SIF still increases, especially for C3 crops. This is attributed to two effects: (1) $\frac{PSII_{\text{yield}}}{SIF_{\text{yield}}}$ of crops varies less than in other ecosystems, since crops in this region rarely experienced severe stress conditions, which would lead to a strong reduction of $\frac{PSII_{\text{yield}}}{SIF_{\text{yield}}}$. Thus, the correspondence between SIF and actual ETR (Ja) is highly linear for crops; (2) Ja:GPP varies between C3 and C4, which is determined by the number of electrons required for carboxylation. The latter consideration also results in a different GPP:SIF relationship between C3 and C4 crops, with a steeper GPP:SIF slope for C4 plants—an important consideration when using SIF as a proxy for crop productivity. A direct comparison of satellite SIF measurements against two flux tower sites in a highly agricultural area in Iowa further supports this finding at larger spatial scales. At the county scale, we found that SIF is highly correlated with crop productivity derived from the USDA NASS database ($R^2 = 0.72$). Using ancillary information on crop-planted fraction and relative C3 crop ratio per county, we can further improve our estimate using a multiple linear regression model to $R^2 = 0.86$. Our model-free SIF-based crop productivity estimation framework appears promising and can provide insights to monitor the crop productivity globally outside the United States, especially in developing agricultural countries. A validation approach against well-documented productivity estimates in the United States represented a necessary proof of concept before applying the method to less well-monitored agricultural areas.

Acknowledgments
Part of this research was funded by the NASA Carbon Cycle Science program (grant NNX17AE14G). L.H. thanks the Resnick Sustainability Institute at Caltech for fellowship support. TROPOMI SIF data generation by P.K. and C.F. is funded by the Earth Science U.S. Participating Investigator program (grant NNX15AH95G). TROPOMI SIF product is available at ftp://fluo.gps.caltech.edu/data/tropomi/. County-level crop statistics is available at the USDA NASS Quick Stats Database (quickstats.nass.usda.gov). Crop-specific land cover data layer CDL can be accessed at https://nassgeodata.gmu.edu/CropScape/.

References

Amthor, J. S. (2012). *Respiration and crop productivity*. Springer Science & Business Media.
Amthor, J. S. (1989). Crop growth and maintenance respiration. In *Respiration and crop productivity*, (pp. 69–104). New York, NY: Springer.
Anderson, M. C., Allen, R. G., Morse, A., & Kustas, W. P. (2012). Use of Landsat thermal imagery in monitoring evapotranspiration and managing water resources. *Remote Sensing of Environment*, *122*, 50–65. https://doi.org/10.1016/j.rse.2011.08.025
Badgley, G., Field, C. B., & Berry, J. A. (2017). Canopy near-infrared reflectance and terrestrial photosynthesis. *Science advances*, *3*(3), e1602244. https://doi.org/10.1126/sciadv.1602244
Baker, J. M., & Griffis, T. J. (2005). Examining strategies to improve the carbon balance of corn/soybean agriculture using eddy covariance and mass balance techniques. *Agricultural and Forest Meteorology*, *128*(3-4), 163–177. https://doi.org/10.1016/j.agrformet.2004.11.005
Burba, G. (2013). *Eddy covariance method for scientific, industrial, agricultural and regulatory applications: A field book on measuring ecosystem gas exchange and areal emission rates*. LI-Cor Biosciences.
Collatz, G. J., Ribas-Carbo, M., & Berry, J. A. (1992). Coupled photosynthesis-stomatal conductance model for leaves of C4 plants. *Functional Plant Biology*, *19*(5), 519–538. https://doi.org/10.1071/PP9920519
Dechant, B., Ryu, Y., Badgley, G., Zeng, Y., Berry, J. A., Zhang, Y., et al. (2019). Canopy structure explains the relationship between photosynthesis and sun-induced chlorophyll fluorescence in crops. https://doi.org/10.31223/osf.io/cbxpq
DeLucia, E. H., Drake, J. E., Thomas, R. B., & Gonzalez-Meler, M. I. Q. U. E. L. (2007). Forest carbon use efficiency: is respiration a constant fraction of gross primary production? *Global Change Biology*, *13*(6), 1157–1167. https://doi.org/10.1111/j.1365-2486.2007.01365.x
Dold, C., Büyükcangaz, H., Rondinelli, W., Prueger, J. H., Sauer, T. J., & Hatfield, J. L. (2017). Long-term carbon uptake of agro-ecosystems in the Midwest. *Agricultural and Forest Meteorology*, *232*, 128–140. https://doi.org/10.1016/j.agrformet.2016.07.012
Dold, C., Hatfield, J. L., Prueger, J. H., Moorman, T. B., Sauer, T. J., Cosh, M. H., et al. (2019). Upscaling Gross Primary Production in Corn-Soybean Rotation Systems in the Midwest. *Remote Sensing*, *11*(14), 1688. https://doi.org/10.3390/rs11141688
Du, S., Liu, L., Liu, X., Guo, J., Hu, J., Wang, S., & Zhang, Y. (2019). SIFSpec: measuring solar-induced chlorophyll fluorescence observations for remote sensing of photosynthesis. *Sensors*, *19*(13), 3009. https://doi.org/10.3390/s19133009
Dutta, D., Schimel, D. S., Sun, Y., van der Tol, C., & Frankenberg, C. (2019). Optimal inverse estimation of ecosystem parameters from observations of carbon and energy fluxes. *Biogeosciences*, *16*(1), 77–103. https://doi.org/10.5194/bg-16-77-2019

Farquhar, G. D., von Caemmerer, S. V., & Berry, J. A. (1980). A biochemical model of photosynthetic CO 2 assimilation in leaves of C 3 species. *Planta*, *149*(1), 78–90. https://doi.org/10.1007/BF00386231

Fischer, R. A. (2015). Definitions and determination of crop yield, yield gaps, and of rates of change. *Field Crops Research*, *182*, 9–18. https://doi.org/10.1016/j.fcr.2014.12.006

Flexas, J., Escalona, J. M., Evain, S., Gulías, J., Moya, I., Osmond, C. B., & Medrano, H. (2002). Steady-state chlorophyll fluorescence (Fs) measurements as a tool to follow variations of net CO2 assimilation and stomatal conductance during water-stress in C3 plants. *Physiologia plantarum*, *114*(2), 231–240.

Frankenberg, C., Fisher, J. B., Worden, J., Badgley, G., Saatchi, S. S., Lee, J. E., et al. (2011). New global observations of the terrestrial carbon cycle from GOSAT: Patterns of plant fluorescence with gross primary productivity. *Geophysical Research Letters*, *38*, L17706. https://doi.org/10.1029/2011gl048738

Frankenberg, C., Pollock, R., Lee, R. A. M., Rosenberg, R., Blavier, J. F., Crisp, D., et al. (2015). The Orbiting Carbon Observatory (OCO-2): spectrometer performance evaluation using pre-launch direct sun measurements. *Atmospheric Measurement Techniques*, *8*(1), 301–313. https://doi.org/10.5194/amt-8-301-2015

Gentine, P., & Alemohammad, S. H. (2018). Reconstructed solar-induced fluorescence: A machine learning vegetation product based on MODIS surface reflectance to reproduce GOME-2 solar-induced fluorescence. *Geophysical Research Letters*, *45*, 3136–3146. https://doi.org/10.1002/2017GL076294

Gitelson, A. A., & Gamon, J. A. (2015). The need for a common basis for defining light-use efficiency: Implications for productivity estimation. *Remote Sensing of Environment*, *156*, 196–201. https://doi.org/10.1016/j.rse.2014.09.017

Grossmann, K., Frankenberg, C., Magney, T. S., Hurlock, S. C., Seibt, U., & Stutz, J. (2018). PhotoSpec: A new instrument to measure spatially distributed red and far-red Solar-Induced Chlorophyll Fluorescence. *Remote Sensing of Environment*, *216*, 311–327. https://doi.org/10.1016/j.rse.2018.07.002

Gu, L., Han, J., Wood, J. D., Chang, C. Y. Y., & Sun, Y. (2019). Sun-induced Chl fluorescence and its importance for biophysical modeling of photosynthesis based on light reactions. *New Phytologist*, *223*(3), 1179–1191. https://doi.org/10.1111/nph.15796

Guan, K., Berry, J. A., Zhang, Y., Joiner, J., Guanter, L., Badgley, G., & Lobell, D. B. (2016). Improving the monitoring of crop productivity using spaceborne solar-induced fluorescence. *Global change biology*, *22*(2), 716–726. https://doi.org/10.1111/gcb.13136

Guan, K., Wu, J., Kimball, J. S., Anderson, M. C., Frolking, S., Li, B., et al. (2017). The shared and unique values of optical, fluorescence, thermal and microwave satellite data for estimating large-scale crop yields. *Remote sensing of environment*, *199*, 333–349. https://doi.org/10.1016/j.rse.2017.06.043

Guanter, L., Zhang, Y., Jung, M., Joiner, J., Voigt, M., Berry, J. A., et al. (2014). Global and time-resolved monitoring of crop photosynthesis with chlorophyll fluorescence. *Proceedings of the National Academy of Sciences*, *111*(14), E1327–E1333. https://doi.org/10.1073/pnas.1320008111

Huete, A., Didan, K., Miura, T., Rodriguez, E. P., Gao, X., & Ferreira, L. G. (2002). Overview of the radiometric and biophysical performance of the MODIS vegetation indices. *Remote sensing of environment*, *83*(1-2), 195–213. https://doi.org/10.1016/S0034-4257(02)00096-2

Jin, Z., Azzari, G., & Lobell, D. B. (2017). Improving the accuracy of satellite-based high-resolution yield estimation: A test of multiple scalable approaches. *Agricultural and forest meteorology*, *247*, 207–220. https://doi.org/10.1016/j.agrformet.2017.08.001

Köhler, P., Frankenberg, C., Magney, T. S., Guanter, L., Joiner, J., & Landgraf, J. (2018). Global retrievals of solar-induced chlorophyll fluorescence with TROPOMI: First results and intersensor comparison to OCO-2. *Geophysical Research Letters*, *45*, 10,456–10,463. https://doi.org/10.1029/2018GL079031

Konings, A. G., Piles, M., Das, N., & Entekhabi, D. (2017). L-band vegetation optical depth and effective scattering albedo estimation from SMAP. *Remote Sensing of Environment*, *198*, 460–470. https://doi.org/10.1016/j.rse.2017.06.037

Lee, J. E., Frankenberg, C., van der Tol, C., Berry, J. A., Guanter, L., Boyce, C. K., et al. (2013). Forest productivity and water stress in Amazonia: Observations from GOSAT chlorophyll fluorescence. *Proceedings of the Royal Society B: Biological Sciences*, *280*(1761), 20130171. https://doi.org/10.1098/rspb.2013.0171

Li, X., & Xiao, J. (2019). A global, 0.05-degree product of solar-induced chlorophyll fluorescence derived from OCO-2, MODIS, and reanalysis data. *Remote Sensing*, *11*(5), 517. https://doi.org/10.3390/rs11050517

Li, X., Xiao, J., He, B., Altaf Arain, M., Beringer, J., Desai, A. R., et al. (2018). Solar-induced chlorophyll fluorescence is strongly correlated with terrestrial photosynthesis for a wide variety of biomes: First global analysis based on OCO-2 and flux tower observations. *Global change biology*, *24*(9), 3990–4008. https://doi.org/10.1111/gcb.14297

Li, Z., Zhang, Q., Li, J., Yang, X., Wu, Y., Zhang, Z., et al. (2020). Solar-induced chlorophyll fluorescence and its link to canopy photosynthesis in maize from continuous ground measurements. *Remote Sensing of Environment*, *236*, 111420. https://doi.org/10.1016/j.rse.2019.111420

Liu, L., Guan, L., & Liu, X. (2017). Directly estimating diurnal changes in GPP for C3 and C4 crops using far-red sun-induced chlorophyll fluorescence. *Agricultural and Forest Meteorology*, *232*, 1–9. https://doi.org/10.1016/j.agrformet.2016.06.014

Lobell, D. B., Hicke, J. A., Asner, G. P., Field, C. B., Tucker, C. J., & Los, S. O. (2002). Satellite estimates of productivity and light use efficiency in United States agriculture, 1982–98. *Global Change Biology*, *8*(8), 722–735. https://doi.org/10.1046/j.1365-2486.2002.00503.x

Lobell, D. B., Thau, D., Seifert, C., Engle, E., & Little, B. (2015). A scalable satellite-based crop yield mapper. *Remote Sensing of Environment*, *164*, 324–333. https://doi.org/10.1016/j.rse.2015.04.021

Magney, T. S., Bowling, D. R., Logan, B. A., Grossmann, K., Stutz, J., Blanken, P. D., et al. (2019). Mechanistic evidence for tracking the seasonality of photosynthesis with solar-induced fluorescence. *Proceedings of the National Academy of Sciences*, *116*(24), 11640–11645. https://doi.org/10.1073/pnas.1900278116

Magney, T. S., Frankenberg, C., Fisher, J. B., Sun, Y., North, G. B., Davis, T. S., et al. (2017). Connecting active to passive fluorescence with photosynthesis: A method for evaluating remote sensing measurements of Chl fluorescence. *New Phytologist*, *215*(4), 1594–1608. https://doi.org/10.1111/nph.14662

Magney, T. S., Frankenberg, C., Köhler, P., North, G., Davis, T. S., Dold, C., et al. (2019). Disentangling changes in the spectral shape of chlorophyll fluorescence: Implications for remote sensing of photosynthesis. *Journal of Geophysical Research: Biogeosciences*, *124*, 1491–1507. https://doi.org/10.1029/2019JG005029

Miao, G., Guan, K., Yang, X., Bernacchi, C. J., Berry, J. A., DeLucia, E. H., et al. (2018). Sun-induced chlorophyll fluorescence, photosynthesis, and light use efficiency of a soybean field from seasonally continuous measurements. *Journal of Geophysical Research: Biogeosciences*, *123*, 610–623. https://doi.org/10.1002/2017JG004180

Mueller, N. D., Butler, E. E., McKinnon, K. A., Rhines, A., Tingley, M., Holbrook, N. M., & Huybers, P. (2016). Cooling of US Midwest summer temperature extremes from cropland intensification. *Nature Climate Change*, *6*(3), 317–322. https://doi.org/10.1038/nclimate2825

Peters, W., Jacobson, A. R., Sweeney, C., Andrews, A. E., Conway, T. J., Masarie, K., et al. (2007). An atmospheric perspective on North American carbon dioxide exchange: CarbonTracker. *Proceedings of the National Academy of Sciences*, *104*(48), 18925–18930. https://doi.org/10.1073/pnas.0708986104

Porcar-Castell, A., Tyystjärvi, E., Atherton, J., Van der Tol, C., Flexas, J., Pfündel, E. E., et al. (2014). Linking chlorophyll a fluorescence to photosynthesis for remote sensing applications: mechanisms and challenges. *Journal of experimental botany*, *65*(15), 4065–4095. https://doi.org/10.1093/jxb/eru191

Running, S. W., Nemani, R. R., Heinsch, F. A., Zhao, M., Reeves, M., & Hashimoto, H. (2004). A continuous satellite-derived measure of global terrestrial primary production. *Bioscience*, *54*(6), 547–560. https://doi.org/10.1641/0006-3568(2004)054[0547:ACSMOG]2.0.CO;2

Ryu, Y., Berry, J. A., & Baldocchi, D. D. (2019). What is global photosynthesis? History, uncertainties and opportunities. *Remote sensing of environment*, *223*, 95–114. https://doi.org/10.1016/j.rse.2019.01.016

Smith, W. K., Biederman, J. A., Scott, R. L., Moore, D. J. P., He, M., Kimball, J. S., et al. (2018). Chlorophyll fluorescence better captures seasonal and interannual gross primary productivity dynamics across dryland ecosystems of southwestern North America. *Geophysical Research Letters*, *45*, 748–757. https://doi.org/10.1002/2017GL075922

Smith, W. K., Cleveland, C. C., Reed, S. C., & Running, S. W. (2014). Agricultural conversion without external water and nutrient inputs reduces terrestrial vegetation productivity. *Geophysical Research Letters*, *41*, 449–455. https://doi.org/10.1002/2013GL058857

Song, L., Guanter, L., Guan, K., You, L., Huete, A., Ju, W., & Zhang, Y. (2018). Satellite sun-induced chlorophyll fluorescence detects early response of winter wheat to heat stress in the Indian Indo-Gangetic Plains. *Global change biology*, *24*(9), 4023–4037. https://doi.org/10.1111/gcb.14302

Sun, Y., Frankenberg, C., Jung, M., Joiner, J., Guanter, L., Köhler, P., & Magney, T. (2018). Overview of Solar-Induced chlorophyll Fluorescence (SIF) from the Orbiting Carbon Observatory-2: Retrieval, cross-mission comparison, and global monitoring for GPP. *Remote Sensing of Environment*, *209*, 808–823. https://doi.org/10.1016/j.rse.2018.02.016

Sun, Y., Frankenberg, C., Wood, J. D., Schimel, D. S., Jung, M., Guanter, L., et al. (2017). OCO-2 advances photosynthesis observation from space via solar-induced chlorophyll fluorescence. *Science*, *358*(6360), eaam5747. https://doi.org/10.1126/science.aam5747

Turner, A. J., Köhler, P., Magney, T. S., Frankenberg, C., Fung, I., & Cohen, R. C. (2019). A double peak in the seasonality of California's photosynthesis as observed from space. *Biogeosciences*, *17*(2), 405–422. https://doi.org/10.5194/bg-17-405-2020

Turner, D. P., Ritts, W. D., Cohen, W. B., Gower, S. T., Running, S. W., Zhao, M., et al. (2006). Evaluation of MODIS NPP and GPP products across multiple biomes. *Remote sensing of environment*, *102*(3-4), 282–292. https://doi.org/10.1016/j.rse.2006.02.017

Van der Tol, C., Berry, J. A., Campbell, P. K. E., & Rascher, U. (2014). Models of fluorescence and photosynthesis for interpreting measurements of solar-induced chlorophyll fluorescence. *Journal of Geophysical Research: Biogeosciences*, *119*, 2312–2327. https://doi.org/10.1002/2014jg002713

Van der Tol, C., Verhoef, W., Timmermans, J., Verhoef, A., & Su, Z. (2009). An integrated model of soil-canopy spectral radiances, photosynthesis, fluorescence, temperature and energy balance. *Biogeosciences*, *6*(12), 3109–3129. https://doi.org/10.5194/bg-6-3109-2009

Verma, M., Schimel, D., Evans, B., Frankenberg, C., Beringer, J., Drewry, D. T., et al. (2017). Effect of environmental conditions on the relationship between solar-induced fluorescence and gross primary productivity at an OzFlux grassland site. *Journal of Geophysical Research: Biogeosciences*, *122*, 716–733. https://doi.org/10.1002/2016JG003580

Wood, J. D., Griffis, T. J., Baker, J. M., Frankenberg, C., Verma, M., & Yuen, K. (2017). Multiscale analyses of solar-induced florescence and gross primary production. *Geophysical Research Letters*, *44*, 533–541. https://doi.org/10.1002/2016GL070775

Yang, K., Ryu, Y., Dechant, B., Berry, J. A., Hwang, Y., Jiang, C., et al. (2018). Sun-induced chlorophyll fluorescence is more strongly related to absorbed light than to photosynthesis at half-hourly resolution in a rice paddy. *Remote Sensing of Environment*, *216*, 658–673. https://doi.org/10.1016/j.rse.2018.07.008

Yang, X., Tang, J., Mustard, J. F., Lee, J. E., Rossini, M., Joiner, J., et al. (2015). Solar-induced chlorophyll fluorescence that correlates with canopy photosynthesis on diurnal and seasonal scales in a temperate deciduous forest. *Geophysical Research Letters*, *42*, 2977–2987. https://doi.org/10.1002/2015GL063201

Yu, L., Wen, J., Chang, C. Y., Frankenberg, C., & Sun, Y. (2019). High-resolution global contiguous SIF of OCO-2. *Geophysical Research Letters*, *46*, 1449–1458. https://doi.org/10.1029/2018GL081109

Yuan, W., Liu, S., Zhou, G., Zhou, G., Tieszen, L. L., Baldocchi, D., et al. (2007). Deriving a light use efficiency model from eddy covariance flux data for predicting daily gross primary production across biomes. *Agricultural and Forest Meteorology*, *143*(3-4), 189–207. https://doi.org/10.1016/j.agrformet.2006.12.001

Zeng, Y., Badgley, G., Dechant, B., Ryu, Y., Chen, M., & Berry, J. A. (2019). A practical approach for estimating the escape ratio of near--infrared solar-induced chlorophyll fluorescence. *Remote Sensing of Environment*, *232*, 111209. https://doi.org/10.1016/j.rse.2019.05.028

Zhang, Q., Zhang, Y., Li, Z., Li, J., & Zhang, X. (2019, July). The Effects of Sun-Viewer Geometry on Sun-Induced Fluorescence and Its Relationship with Gross Primary Production. In IGARSS 2019-2019 IEEE International Geoscience and Remote Sensing Symposium (pp. 9048-9051). IEEE. https://doi.org/10.1109/IGARSS.2019.8898345

Zhang, Y., Guanter, L., Berry, J. A., Joiner, J., van der Tol, C., Huete, A., et al. (2014). Estimation of vegetation photosynthetic capacity from space-based measurements of chlorophyll fluorescence for terrestrial biosphere models. *Global change biology*, *20*(12), 3727–3742. https://doi.org/10.1111/gcb.12664

Zhang, Y., Joiner, J., Alemohammad, S. H., Zhou, S., & Gentine, P. (2018). A global spatially contiguous solar-induced fluorescence (CSIF) dataset using neural networks. *Biogeosciences*, *15*(19), 5779–5800. https://doi.org/10.5194/bg-15-5779-2018

Zhang, Y., Xiao, X., Jin, C., Dong, J., Zhou, S., Wagle, P., et al. (2016). Consistency between sun-induced chlorophyll fluorescence and gross primary production of vegetation in North America. *Remote Sensing of Environment*, *183*, 154–169. https://doi.org/10.1016/j.rse.2016.05.015

Zhao, M., Heinsch, F. A., Nemani, R. R., & Running, S. W. (2005). Improvements of the MODIS terrestrial gross and net primary production global data set. *Remote sensing of Environment*, *95*(2), 164–176. https://doi.org/10.1016/j.rse.2004.12.011

Zuromski, L. M., Bowling, D. R., Köhler, P., Frankenberg, C., Goulden, M. L., Blanken, P. D., & Lin, J. C. (2018). Solar-induced fluorescence detects interannual variation in gross primary production of coniferous forests in the Western United States. *Geophysical Research Letters*, *45*, 7184–7193. https://doi.org/10.1029/2018GL077906